Gasification of Spent Alkylation Sulfuric Acid Droplets in Hot Environments

Difei F. Wang, Benjamin D. Shaw, and Albert Yang
Mechanical and Aeronautical Engineering Dept., University of California, Davis, CA 95616

Experimental results on gasification behaviors of freely-falling spent alkylation sulfuric acid droplets in high-temperature environments are presented, as well as baseline data on evaporation of water droplets and sulfuric acid droplets. Low evaporation constants have been measured for sulfuric acid droplets and spent acid droplets (relative to water droplets). Shape distortions and fragmentation (microexplosions) of spent acid droplets were also observed, and it has been found that initial droplet diameters are important in determining onset times and intensities of microexplosive behaviors. Simplified theory is developed, which suggests that the droplet distortion and fragmentation behaviors may be a result of SO_2 bubble formation inside the droplets.

Introduction

Spent acids are corrosive byproducts of the petrochemical industry. In the U.S. the refining industry produces more than about 10^8 kg of spent acid every year (Bush and Levine, 1992). One important class of spent acid is spent alkylation sulfuric acid, which is the focus of this article. In this article spent alkylation sulfuric acid will be referred to simply as spent acid. The range of spent acid grades produced is wide, ranging from dilute to comparatively concentrated forms, which may be lightly or heavily contaminated with organic and inorganic impurities. Because of increasing concerns about pollution control, greater attention has been placed on reprocessing (regenerating) spent acid. There is significant interest to increase process safety and decrease process costs in spent acid regeneration systems.

Thermal decomposition of spent acid into sulfur dioxide, where the SO_2 is subsequently converted to commercial sulfuric acid and oleum, is a common method of regenerating spent acid containing organic impurities. The most expedient methods of thermal decomposition are low-temperature (973–1,073 K) decomposition in a fluidized bed and high-temperature (1,273–1,473 K) splitting (Krasil'nikov et al., 1990). The high-temperature method has the advantage that organic impurities are oxidized simultaneously, and the fresh acid produced from SO_2 remains free of any organic impurities. However, this process involves high temperatures, complicating the maintenance of the equipment and requiring significant energy expenditures.

A major problem in high-temperature spent acid decomposition is that droplet residence times within high-temperature zones inside furnaces are limited. This can lead to formation of particulates that can accumulate within a regeneration system. Droplets can also accumulate in pools at the bottom of a furnace, although this seldom occurs in practice. Therefore, it is very important to understand the gasification mechanisms of spent acid droplets in order that such problems may be prevented. It is extremely difficult to perform experiments directly in a full-scale industrial furnace. Large-scale numerical simulation provides some understanding of the flow and temperature fields inside an industrial furnace; however, prediction of the gasification behaviors of spent acid sprays is not feasible without fundamental data on gasification behaviors of spent acid droplets. To assist in developing spray models, as well as to increase understanding of fundamental spent acid droplet behaviors, this article presents experimental results on gasification of spent acid droplets in hot environments. Simplified theory is also presented to estimate the influence of SO_2 formation in the liquid phase on distortion and fragmentation of spent-acid droplets. It is noted that while numerous articles have been published in the general area of droplet gasification, no publications have been found

Correspondence concerning this article should be addressed to B. D. Shaw.
Current address of D. F. Wang: Cheng Power Systems, Inc., 480 San Antonio Road, Suite 120, Mountain View, CA 94040.
Current address of A. Yang: Rhodia, 8615 Manchester Boulevard, Houston, TX 77012.

which relate specifically to sulfuric acid droplets or spent acid droplets.

The present investigation explores the gasification characteristics of freely-falling droplets of spent acid falling in environments of controlled temperature and composition. For comparison, experiments were also performed with droplets of water, as well as with sulfuric acid droplets. Because spent acid is corrosive and difficult to work with, the simplest method of performing droplet experiments is to use the fiber-supported droplet technique, that is, where a droplet is supported at the end of a fiber and immersed in a hot gaseous environment. In preliminary experiments with fiber-supported spent acid droplets, it was found that the fibers seemed to strongly influence gasification behaviors (for example, by inducing bubble formation and growth inside droplets, producing strong shape distortions and ''microexplosions,'' that is, droplet shattering). Because of such behaviors, experiments with droplets freely-falling in hot environments were performed instead. In the present experiments, monodisperse droplet streams were injected and gasified within the high-temperature environment of a constant cross-sectional-area flow tube. As described later in this article, it was found that spent acid droplets vaporized quite slowly relative to water droplets, and the spent acid droplets displayed distortion and fragmentation (microexplosive) behaviors, which changed as the initial droplet size was varied. Simplified theory suggests that the distortion and fragmentation of spent acid droplets may result from generation and growth of SO_2 bubbles within the droplets.

It is also noted that this investigation provides useful information on behaviors of multicomponent fuel droplets under well-controlled conditions. Practical fuels are generally blends that contain both low- and high-volatility components. In practice, it is found that the high-volatility components gasify first, with liquid-phase behaviors eventually being controlled by the lower-volatility components left behind in the droplets. In previous research (for example, Aharon and Shaw, 1998), significant efforts have been directed toward utilizing reduced gravity to perform fundamental experiments with bicomponent droplets, where the droplet components have widely different volatilities. The present experiments with spent acid extend this previous research in the sense that spent acid boiling temperatures are much higher than encountered with typical engine fuels (though not necessarily oil-fired burner fuels). This has allowed observation of how having one component with an extremely-high boiling point influences gasification rates and microexplosive behaviors.

Experimental Methodology

Figure 1 shows the experimental setup. There are many concerns in the design and operation of laboratory-scale experiments with acids or spent acids. These materials are dangerous, and appropriate precautions must be taken by anyone working with them. For example, spent acid is highly reactive and corrodes many metals and most adhesives. Significant efforts have been made in these experiments to design devices that generate monodisperse sulfuric acid droplet streams. Descriptions of the experimental setup are provided below.

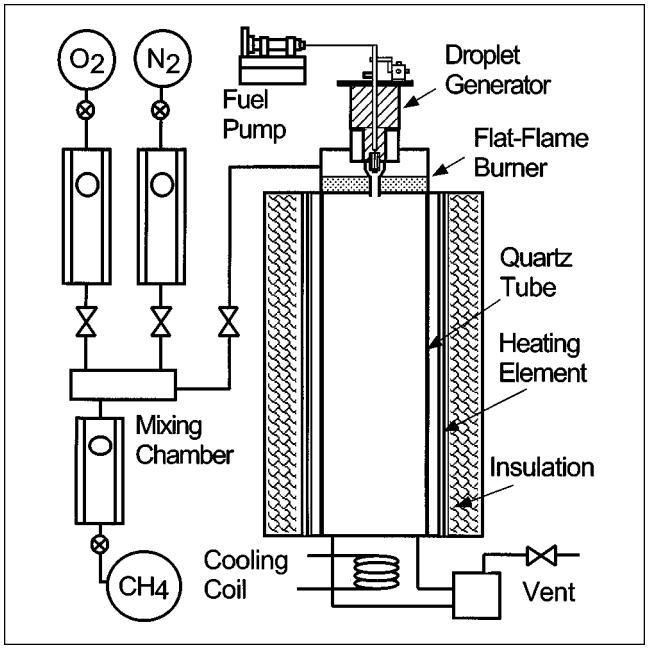

Figure 1. Drop-tube experimental system.

Monodisperse droplet stream generation

Droplets were generated with a specially-designed aerodynamic droplet generator, as shown in Figure 2. This aerodynamic droplet generator is an adaptation of the design by Green et al. (1989), and features droplet production by the application of aerodynamic principles. The liquids were slowly pumped by a syringe pump through a capillary tube, and were disengaged as droplets when the surface tension holding the liquid at the capillary tip was overcome by the drag force of the coaxial gas flow (which was N_2). This droplet generator could produce uniformly-sized droplets of about 300–700 μm, spaced greater than 60 droplet diameters. It is noted that

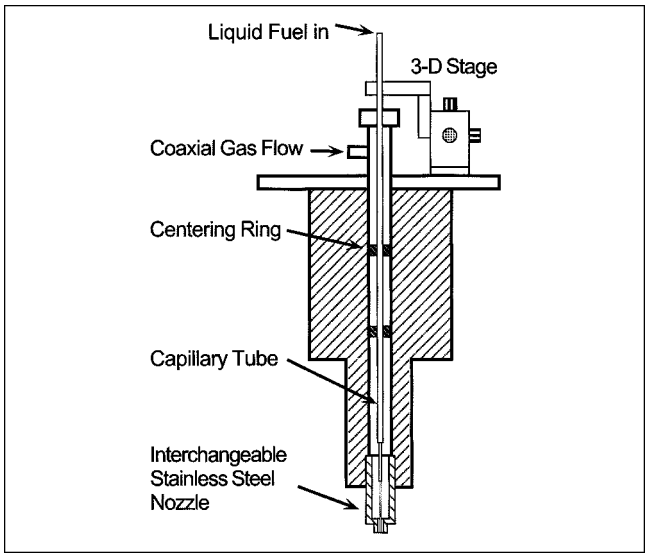

Figure 2. Aerodynamic droplet generator.

droplets of present commercial interest are typically smaller than 300 μm. However, because of limitations of the droplet generator, it was not possible to work with droplets initially smaller than about 300 μm.

The frequency of droplet generation was controlled by the outside diameter of the capillary tube and the stripping gas-flow rate. The design of the stainless steel interchangeable nozzle made it possible to generate stable monodisperse droplet streams for a variety of liquid samples. It also significantly reduced corrosion damage from sulfuric acid and spent acid.

High-temperature environment

It is very important to produce controlled high-temperature environments for droplet gasification studies. For this purpose, the post-combustion gases from an inverted flat-flame burner were used to produce a high-temperature flow in a quartz tube with a circular cross section (75 mm ID, 800 mm length). The temperatures and compositions of the droplet environments were controlled by varying the composition of the premixed gas fed to the flat-flame burner, the burner cooling rates, and the power input to heating elements surrounding the quartz tube. The carrier gases were selected to be similar to ranges that exist in practical spent acid recovery furnaces (Albright and Lang, 1996). Based on equilibrium calculations, the carrier gas major species were calculated to be O_2, CO_2, N_2, and H_2O with the mole fractions $X_{O_2} = 0.037$, $X_{CO_2} = 0.145$, $X_{N_2} = 0.527$, and $X_{H_2O} = 0.291$. Except where explicitly noted, these mole fractions apply to the experiments discussed in this article.

Two half-section heating elements were installed around the quartz tube as an auxiliary heating source other than the flat-flame burner to assure high-temperature flow along the entire test section. Figure 3 is a plot of temperature profiles measured with thermocouples for two typical flow conditions with inlet gas temperatures of 1,200 and 1,400 K. Results in Figure 3 indicate that the centerline gas-temperature distributions are not uniform for the entire tube. This is partially

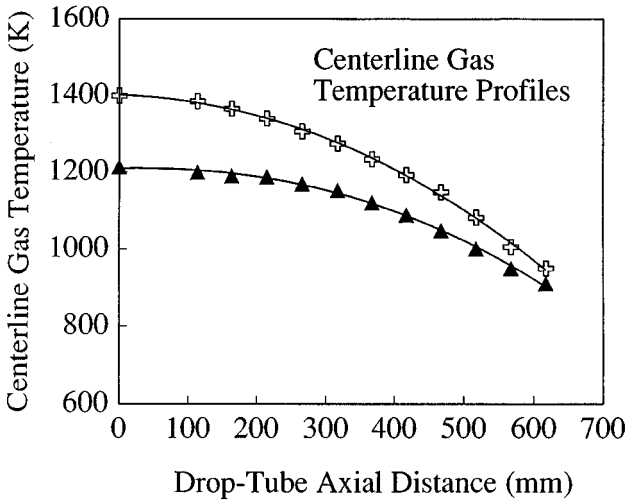

Figure 3. Centerline gas-flow temperature distributions for inlet gas temperatures of 1,200 K and 1,400 K.

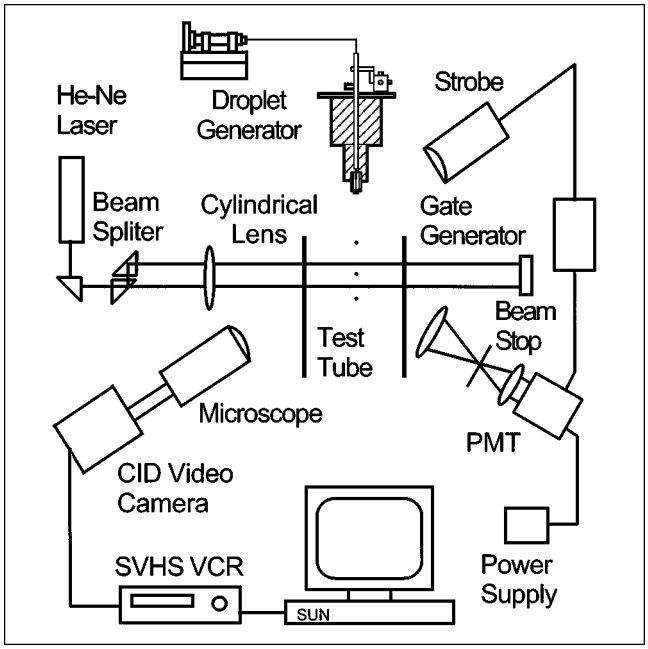

Figure 4. Optical measurement and signal processing systems.

because the insulation was not thick enough to allow the heating elements to reach surface temperatures higher than 1,173 K; the insulation thickness was limited because a long-distance microscope used to image droplets had to remain outside the insulation, and this microscope also had to be within a certain distance to allow droplets to be imaged. Another reason is that a cooling assembly at the bottom of the furnace increased the local heat losses near its location. The drop tube axial distance of 600 mm in Figure 3 corresponds to droplet residence times of about 300 ms.

Optimal measurement and data acquisition systems

The optical measurement and image processing system is shown in Figure 4. A He-Ne laser beam and a photo-multiplier tube (PMT) were used to detect passing droplets. *In-situ* imaging of droplets was accomplished with a Mono-Zoom 7 microscope, a high resolution CID video camera, and a super-VHS VCR. Backlighting was provided by a strobe. The strobe was triggered to flash when a droplet passed through the focal point of the laser beam. The PMT system and the laser beam were aligned, and the PMT system was focused on the focal point of the laser beam. Adjustment of the vertical position of the entire furnace (including the flat-flame burner and the quartz tube) relative to the optical system permitted imaging at different heights along the quartz drop tube so that droplet sizes, shapes, and velocities could be monitored and recorded as functions of residence time.

Droplet velocities were measured along the length of the drop tube. Two laser sheets, separated by 2 mm (center-to-center), were formed using a beam splitter and a cylindrical lens. As a droplet passed through the sheets, two Gaussian-shaped spikes occurred on the photomultiplier output signals. Droplet velocities were then calculated by dividing the distance between the two laser sheets by the time between

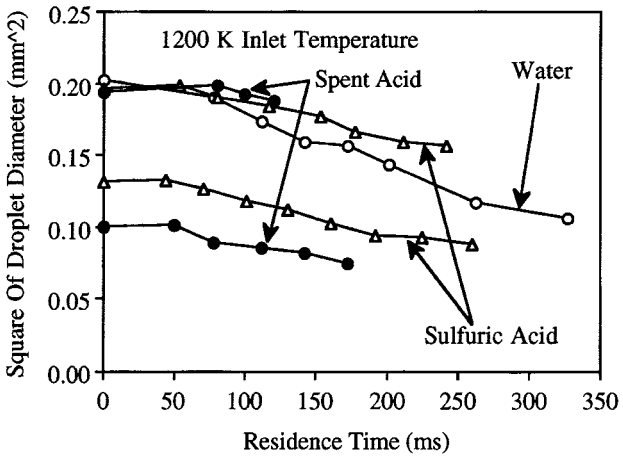

Figure 5. Temporal variations of the square of the droplet diameter for water droplets, sulfuric acid droplets, and spent alkylation sulfuric acid droplets in the drop tube with inlet gas temperatures of 1,200 K.

All data shown were obtained by averaging diameter data from several droplets at each drop tube location.

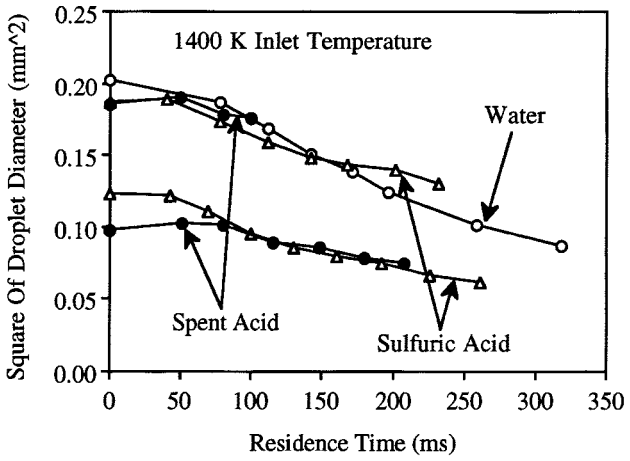

Figure 6. Temporal variations of the square of the droplet diameter for water droplets, sulfuric acid droplets, and spent alkylation sulfuric acid droplets in the drop tube with inlet gas temperatures of 1,400 K.

All data shown were obtained by averaging diameter data from several droplets at each drop tube location.

the spike centers. The instantaneous values of the reciprocal of the velocity were then integrated over the distance along the drop tube to calculate droplet residence times. In general, droplet-gas relative velocities were in the 1–2 m/s range, and droplet-gas relative velocity profiles were quite similar for all of the droplets studied.

Analysis of droplet images was performed using digital image analysis. In performing these analyses, images were input from the video tape into a Sun Sparcstation 2 work station and digitized by a Video Pix board. The images were stored with 8 bit resolution. The data were analyzed using the commercial image-processing software C-Vista (Sigel, 1992), and digital filters were sometimes used to enhance edges and facilitate processing of the images. A fine metal wire (254 μm in diameter) was used to calibrate the measurements. During the analysis of a droplet, discrete points were manually selected along the droplet surface. These points were used to define a circle of best fit that passed through them. The diameter of this circle was assumed to be the droplet diameter, and the center (centroid) of this circle was assumed to be the droplet center. These processes were repeated several times, and average values were taken. Only droplets that were very close to being spherical were analyzed in this fashion. Droplet diameters were not evaluated for droplets that were significantly distorted.

Results and Discussion

Evaporation of water droplets and sulfuric acid droplets

The purpose of these experiments was to provide base line data on evaporation of water and sulfuric acid droplets for comparison with experiments on spent acid droplets. Figures 5 and 6 show the squares of the droplet diameters (d) vs. time (t) for water droplets with inlet gas temperatures of 1,200 and 1,400 K, respectively. The results show that after an initial period associated with droplet heating, the d^2-t curves (where d is droplet diameter and t is time) are essentially linear for pure water. The average evaporation rate constants K [where $K = -d(d^2)/dt$] were also determined from the present experimental data using a linear least-squares curve fit. These K values are listed in Table 1. All K values listed in this table (that is, for all droplet compositions) were calculated by excluding any initial periods of droplet heating. Using analyses described elsewhere (Wang and Shaw, 1996), uncertainties in the K values are estimated to be about $\pm 10\%$.

Table 1. Evaporation Rate Constants of Pure Water, Pure Sulfuric Acid, and Spent Alkylation Sulfuric Acid Droplets*

Inlet Gas Temp. (K)	H_2O	H_2SO_4	H_2SO_4	Spent Acid
1,200	$K = 0.31$ mm^2/s $d_0 = 450$ μm $t_e = 0.65$ s	$K = 0.23$ mm^2/s $d_0 = 442$ μm $t_e = 0.85$ s	$K = 0.21$ mm^2/s $d_0 = 362$ μm $t_e = 0.62$ s	$K = 0.19$ mm^2/s $d_0 = 315$ μm $t_e = 0.52$ s
1,400	$K = 0.42$ mm^2/s $d_0 = 440$ μm $t_e = 0.46$ s	$K = 0.30$ mm^2/s $d_0 = 432$ μm $t_e = 0.62$ s	$K = 0.27$ mm^2/s $d_0 = 350$ μm $t_e = 0.45$ s	$K = 0.20$ mm^2/s $d_0 = 312$ μm $t_e = 0.49$ s

*The variable K is the evaporation rate constant based on the droplet diameter, d_0 is the initial droplet diameter, and t_e is the projected evaporation time based on K and d_0. Evaporation times, which were simply estimated as $t_e = d_0^2/K$, assume that droplet fragmentation does not occur.

Figures 5 and 6 also show plots of the temporal variations of the square of the droplet diameter vs. time for initially-pure sulfuric acid droplets (99.5% purity by weight). The results show that the d^2-t curves exhibit nearly constant or slightly increasing diameters near the beginning, followed by decreases in droplet diameters. In addition, K values were substantially smaller than for the water droplets (see Table 1). Estimates indicate that the low K values may be a result of the fact that sulfuric acid has a very high boiling point relative to water (it is also noted that endothermic decomposition of sulfuric acid in the gas phase might further reduce vaporization rates). Before a droplet can vigorously gasify, its surface must be heated to temperatures approaching the liquid saturation temperature in order that a sufficiently-high vapor pressure will exist. The boiling point of pure sulfuric acid at 0.1 MPa is listed as being about 553 K (Müller, 1994). However, sulfuric acid can absorb water from the gas phase, which can appreciably increase the boiling point to about 600 K even if only small amounts of water are present in the liquid phase (Donovan and Salamone, 1978). Characteristic times to heat surfaces of 300–400 μm sulfuric acid droplets (immersed in 1,200–1,400 K environments) from 300 K to about 600 K are in the 100–250 ms range when evaporation is neglected; mass transfer from the surface of a droplet will increase these heating times somewhat. It is noted that these heating times are of the order of the residence times that could be attained in the present experiments. For comparison, characteristic times to heat the surfaces of water droplets of the sizes considered in these experiments from 300 K to 373 K are approximately 25 ms when evaporation is neglected.

It is noted that liquid mixtures of water and sulfuric acid can form an azeotrope, which has a boiling point maximum (Donovan and Salamone, 1978). This azeotrope would be stable in the sense that the droplet composition would approach this azeotropic state with time. Based upon available data (Donovan and Salamone, 1978), it is likely that a sulfuric acid droplet in the present experiments, which is at this azeotropic state, would be mostly composed of sulfuric acid, and that the saturation temperature for the mixture at the droplet surface could be as high as about 603 K. In order to predict the azeotropic state that a gasifying sulfuric acid droplet might approach, it is necessary to model transient heat and mass transfer in both the liquid and gas phases. In addition, significant gas-phase chemistry will occur at sufficiently-high temperatures, where the H_2SO_4 will first decompose into primarily H_2O and SO_3, and the SO_3 will then decompose into SO_2 and O_2. Some of the H_2O that is produced in these reactions (as well as H_2O already present in the ambient) can be transported back to the droplet surface, where it can be absorbed into the liquid phase. This absorbed H_2O will diffuse into the droplet interior and will also alter the partial pressures for the components at the liquid surface. To properly account for all of these effects would require a complex computational model. The development of such a model is a major effort, and is beyond the scope of the present investigation.

In general, the sulfuric acid droplet images indicated that there was some small droplet distortion during the early stages of evaporation, and that droplet fragmentation never occurred within the drop tube. The results suggest that a much longer tube is needed to complete the evaporation process for sulfuric acid droplets with initial diameters of about 300 μm or larger. Because of the limitations of the droplet generator, smaller droplets were not investigated to determine if K values would increase at late times in the gasification history as sulfuric acid droplets become smaller and droplet heating becomes less important.

Gasification and microexplosion of spent alkylation sulfuric acid droplets

The compositions of spent alkylation sulfuric acid mixtures are complex and sometimes not well characterized. The sample we used in our tests was the refinery stream product from a petroleum company. The material safety data sheet listed the ingredients as 85–95% sulfuric acid, 5–15% hydrocarbons, and catalytic alkylation byproducts, and 0–5% water. During thermal decomposition of sulfuric acid wastes, complex processes occur in the liquid droplets. For example, it has been established that H_2O and SO_2 are formed in liquid spent acids at rates that increase as the liquid temperature is increased (Sung et al., 1993); various hydrocarbon species, tarlike materials, and carbon particles can be formed as well (Sung et al., 1993). These species can potentially affect spent acid droplet behaviors. It is also noted that the boiling temperature listed for the spent acid was quite high (552 K) such that droplet heating was likely important over the available residence times.

Droplet distortion and fragmentation (microexplosions) occurred for spent acid droplets in the experiments. These phenomena were very likely a result of gas bubble formation and growth within the droplets. Figures 5 and 6 show d^2-t data for time periods when distortion and fragmentation were negligible. For spent acid droplets with initial droplet diameters around 440 μm and an inlet gas temperature of 1,200 K, droplet shape distortions first appeared at about 120–140 ms. Droplet behaviors at this stage were characterized by a sudden buildup of vapor within the droplets, leading to expansion and distortion of the droplets. Swelling of a vapor-filled droplet occurred until the droplet surface ruptured, resulting in fragmentation at about 180 ms. The droplets were not strongly shattered as a result of fragmentation; the parent droplets could fragment into two or more droplets of significant sizes. The shape-distortion behaviors could be a result of SO_2 formation in the liquid phase; SO_2 is not highly soluble in sulfuric acid (Hayduk et al., 1988), and could potentially nucleate bubbles at high enough concentrations. Alternatively, light hydrocarbons or water trapped in the droplets could be raised above a nucleation temperature and could form bubbles. Since distortion and fragmentation happened in the early stages of the evaporation history before significant droplet-size reductions occurred, it was difficult, based on droplet-size measurements, to estimate evaporation rate constants for these droplets. As a result, evaporation rate constant data for 440 μm droplets are not shown in Table 1.

Video image data were also evaluated for 430 μm spent acid droplets with an inlet gas temperature of 1,400 K. In these experiments, droplet-shape distortions were first observed at residence times of about 100–120 ms. Relative to the 440 μm spent acid droplets in 1,200 K ambients, these droplets appeared to undergo stronger fragmentation. Simi-

lar to the 440 μm droplets described above, droplet-shape distortion and fragmentation in the initial stages of the evaporation processes made it difficult to estimate evaporation rate constants based on droplet-size measurements for the 430 μm droplets, so data are not provided in Table 1 for these droplets.

Video images were also processed for spent acid droplets initially about 315 μm in diameter with an inlet gas temperature of 1,200 K. Results indicated that unlike the larger spent acid droplets, there was no distortion until residence times between about 170–200 ms, with sudden and strong fragmentation occurring at about 200 ms. Video images of spent acid droplets (initially 312 μm) with an inlet gas temperature of 1,400 K also revealed similar behaviors with strong fragmentation suddenly occurring at about 210 ms. For these tests with smaller spent acid droplets, evaporation rate constants K could be determined by fitting straight lines with least-squares fits through the d^2-t data up to the state of droplet distortion because the droplets exhibited significant size changes prior to the onset of distortion and fragmentation (the d^2-t data are shown in Figures 5 and 6). The evaporation rate constants determined for inlet gas temperatures of 1,200 and 1,400 K were 0.19 and 0.20 mm^2/s, respectively. These evaporation rate constants are substantially smaller than for the water droplets, but are only somewhat smaller than for the sulfuric acid droplets. Because boiling points for the spent acid droplets are in the same range as sulfuric acid droplets (at least initially), the low K values observed for the spent acid droplets are likely a result of droplet heating, though it is noted that droplet-internal chemistry, and possibly the buildup of heavy hydrocarbon species at the droplet surface, could have played roles as well.

It is briefly mentioned that a series of experiments with spent acid droplets in different gas compositions and environmental temperatures was performed. It appeared in the experiments that organic impurities in the spent acid droplets underwent decomposition; as suggested by visual observation, species in the droplets were converted to solid particles under certain conditions. The combustion of these particles (which were likely mostly carbon) near the bottom of the furnace was observed when the flow temperature in that region was greater than about 1,000 K, and the oxygen concentration of the post-combustion products was over 10% on a molar basis; at lower oxygen concentrations, particle oxidation was not observed. This particle combustion appeared visually as oxidation on the particle surfaces (with the surfaces glowing orange). It is noted that experiments on spent acid decomposition in a fluidized-bed reactor operating at 973 K also confirmed the formation of solid particles (Krasil'nikov et al., 1991). The appearance of solid particles is in accordance with other data (for example, Sung et al., 1993), which indicate that formation of tarlike particles or carbon particles can be expected in spent alkylation sulfuric acid decomposition.

Estimates of the potential role of SO_2 formation on distortion and fragmentation of spent acid droplets

The distortion and fragmentation behaviors of the spent acid droplets were very likely a result of gas generation within the droplets. Liquid water or light hydrocarbons within the droplets could have nucleated, producing bubbles. Alternatively, SO_2 produced within the droplets might have exceeded solubility limits and produced bubbles. This possibility is considered here.

Sung et al. (1993) have shown that SO_2 is formed in spent acid at rates that increase rapidly as the liquid temperature increases. In addition, Hayduk et al. (1988) have published data on SO_2 solubility limits in aqueous sulfuric acid solutions; these data show that SO_2 solubility limits decrease appreciably as the liquid temperature is increased. It is plausible that spent acid droplets, which are decomposing in a hot environment, may attain conditions where SO_2 produced in the liquid phase sufficiently exceeds solubility limits such that bubbles might form; these bubbles could distort and fragment droplets if the bubbles grow sufficiently rapidly.

The kinetics of SO_2 formation are not precisely known, though Sung et al. (1993) have published some data. In their research, Sung et al. studied SO_2 formation rates in spent alkylation sulfuric acid at constant temperatures which ranged from 283–333 K. They found that at a constant temperature T, the wt. % (Y) of SO_2 evolved over the time τ was approximately described by

$$Y \approx k\tau^{1/2} \tag{1}$$

where $k = Ae^{-E/(RT)}$ is a rate constant (A is a pre-exponential factor, E is an activation energy, and R is the universal gas constant). Sung et al. (1993) reported that $E = 8{,}400$ cal/(mol·K) is a typical value applicable to spent alkylation sulfuric acid; this value for E is large enough that k values are predicted to vary significantly with temperature over the liquid temperature ranges of interest here.

In the spent acid droplet experiments performed here, the droplets had variable temperatures such that Eq. 1 is not strictly applicable. However, Eq. 1 can be used to estimate the temperature dependences of characteristic times for SO_2 levels to reach sufficiently-high levels in the liquid such that SO_2 bubble nucleation might occur. In making these estimates, it is assumed that Eq. 1 is valid at temperatures up to the listed boiling point of the spent acid (552 K).

Rearranging Eq. 1 yields

$$\tau \approx (Y/k)^2. \tag{2}$$

Equation 2 can be used to estimate the characteristic time τ for a specified value Y to be attained at a given liquid temperature T. For bubbles to form, Y must exceed the solubility limit. Because the amount by which Y must exceed the solubility limit depends upon the characteristics of the liquid (such as the liquid composition and whether there are nucleation sites present), and these quantities are not well characterized for the present experiments, estimates will be made using Eq. 2 for various assumed values of SO_2 supersaturation (S) in the liquid phase.

Unfortunately, data have not been found for SO_2 solubility limits in spent acid. However, solubility limit data for SO_2 in aqueous sulfuric acid mixtures has been published (Hayduk et al., 1988); the data will be assumed to characterize SO_2 solubility behaviors in spent acid. The data of Hayduk et al. (1988) show that on a mole-fraction basis, the temperature-dependence of the solubility limits X of SO_2 in aqueous sulfuric acid mixtures can be well-approximated by the func-

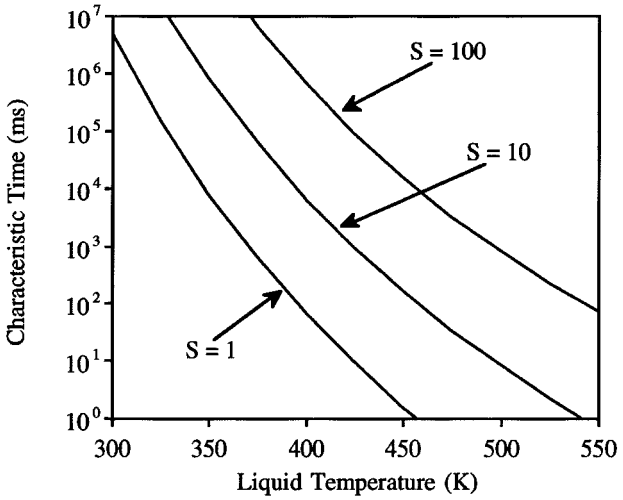

Figure 7. Characteristic times (τ) estimated using Eq. 3 for the onset of SO_2 bubble formation for supersaturation (S) values of 1, 10 and 100.

tional form $X \approx \phi e^{\theta/T}$, where ϕ and θ are constants which can vary somewhat with the liquid composition. The relationship between the mass fraction Y at the onset of bubble formation and the solubility-limit mole fraction X is described by $Y \approx SXW_{SO_2}/W_{ave}$, where W_{SO_2} and W_{ave} are the molecular weight of SO_2 and the average molecular weight of the liquid, respectively, and the supersaturation S has been introduced to allow for SO_2 supersaturation in the liquid. Using the above variables in Eq. 2 results in the following equation for estimation of characteristic times to reach conditions for the onset of bubble formation

$$\tau \approx \left(\frac{S\phi W_{SO_2}}{AW_{ave}}\right)^2 \exp\left[2\left(\theta + \frac{E}{R}\right)\Big/T\right] \qquad (3)$$

In Eq. 3, the group of terms $2(\theta + E/R)/T$ is calculated to be large relative to unity indicating that Eq. 3 will be sensitively dependent upon the temperature, that is, characteristic times for the onset of bubble formation will decrease rapidly as T is increased.

Based upon available data (Sung et al., 1993; Hayduk et al., 1988), appropriate (average) values for use in Eq. 3 are estimated to be as follows: $\phi = 7.9\times10^{-6}$, $\theta = 2{,}505$ K, $E =$ 35,170 kJ/kmol, and $A = 403\ s^{-1/2}$. In addition, the molecular weights $W_{SO_2} = 64$ and $W_{ave} = 100$ are also used. Shown in Figure 7 are values of τ calculated using these numerical values. Because the level of supersaturation required to nucleate bubbles is not known, S was varied over the range 1–100. The upper limit of 100 was selected based upon data for homogeneous nucleation limits of gases in solution (Rubin and Noyes, 1987, 1992). The results in Figure 7 show that characteristic times for the onset of bubble formation depend strongly upon the liquid temperature; variations of several orders of magnitude are evident as the temperature is varied from 300 K to 550 K.

Distortion and fragmentation of 430 and 440 μm spent acid droplets generally occurred 100–120 ms after the droplets were injected. From Eq. 3 or Figure 7, it is estimated that droplet temperatures must be higher than about 400 K if SO_2 nucleation is to occur for $\tau \approx 100$ ms, that is, for $S > 1$ to be achieved with $\tau \approx 100$ ms. Using simple heat-transfer models, average temperatures were estimated for the 430 and 440 μm droplets 100–120 ms after injection. Because the gasification rates of these droplets were not large, convective heat-transfer coefficients were estimated from standard correlations for heat transfer to spheres. Estimates indicated that Biot numbers for the droplets were small relative to unity, and as a result, a lumped-capacitance method was used to estimate droplet temperatures. Average temperatures of the 430 and 440 μm droplets were estimated to be higher than 400 K after about 100–120 ms, indicating that SO_2 bubble nucleation cannot be ruled out as a mechanism for inducing distortion and fragmentation in these droplets. In making these estimates, radiant heat transfer to droplets was estimated to not be dominant in our reactor and was therefore neglected. Allowing for radiant heat transfer will increase estimated droplet temperatures somewhat. It is also noted that radiant heat fluxes may be more significant in commercial reactors than in our laboratory reactor.

The initially-smaller spent acid droplets (312 and 315 μm) did not show distortion and fragmentation behaviors until later in their histories, that is, until about 170–200 ms had elapsed (see Figures 5 and 6). This is surprising because the smaller droplets would likely have experienced faster heating rates than the 430 and 440 μm spent acid droplets. Faster heating rates could cause different chemical-kinetic mechanisms to become dominant, which might lead to different behaviors. For example, at higher heating rates, the smaller droplets might be rapidly heated to temperatures which would favor the production of products other than solid particles. This would promote the attainment of higher supersaturations in droplets by suppressing heterogeneous nucleation. This can account for the stronger fragmentations observed with the smaller droplets as well as the later distortion and fragmentation times. It is worth mentioning that Sung et al. (1993) have presented discussion of various chemical reactions that can occur in spent acid; unfortunately, they also indicate that rates of most of the possible reactions in spent acid have not yet been measured.

Finally, it is noted that Eq. 3 predicts S roughly in the range 50–100 for τ in the range 170–200 ms and liquid temperatures that are approaching the boiling point of spent acid (see Figure 7). These S values are in the range of data of Rubin and Noyes (1987, 1992) for maximum supersaturation values measured at the homogeneous nucleation limits of gases dissolved in liquids. While the mixtures investigated by Rubin and Noyes (1987, 1992) are different than those studied here, the largest S values estimated to apply to the present experiments are intriguingly close to the maximum supersaturations measured by Rubin and Noyes, suggesting that homogeneous nucleation may have been dominant in the present experiments with initially-smaller droplets.

Summary

A drop tube system has been successfully used to study gasification of freely-falling water droplets, sulfuric acid droplets, and spent alkylation sulfuric acid droplets. Microex-

plosions of spent acid droplets were observed; it was found that initial droplet diameters were important in determining shape distortion and microexplosive behaviors of spent acid droplets. It was also found that evaporation rate constants of sulfuric acid droplets and spent acid droplets were significantly lower than for water droplets; this is likely a result of droplet heating effects and possibly endothermic gas-phase chemistry. Simplified theory was developed which suggests that the droplet distortion and fragmentation behaviors may be a result of SO_2 bubble formation inside the droplets. As the droplets heat, SO_2 is formed at rapidly increasing rates and solubility limits of SO_2 likely decrease significantly, leading to conditions which could lead to formation of SO_2 bubbles inside the droplets.

This research has provided a better understanding of spent acid droplet behaviors and of multicomponent droplet behaviors in general, especially for the situation where at least one of the droplet components has an exceedingly-high boiling point. The research has also provided useful data for large-scale numerical simulations, which should aid in improving operations in industrial furnaces. Further experiments and analyses should be performed to increase understanding of the gasification characteristics and chemical-kinetic decomposition mechanisms of spent acid droplets. For example, studies should be performed which focus on droplet fragmentation. Experiments could be performed to determine size distributions of droplets after fragmentation, and also to determine the environmental conditions which optimize fragmentation. It would be interesting to increase initial droplet temperatures (such as by heating the droplet generator), which would allow investigations of later periods in droplet histories by reducing the duration of the initial droplet heatup period. It would also be worthwhile to study the factors affecting conversion of droplet materials into solid particulates. In addition to providing scientific information, this would be of significant industrial value.

Finally, several assumptions were made while developing Eq. 3, and that it would be worthwhile to justify these assumptions. For example, data are needed on the solubility of SO_2 in spent acid, and the effects of finite-rate heating of droplets (such as on chemical-kinetic mechanisms) should be evaluated. In addition, the energetics of liquid-phase chemistry have not been taken into account, and Eq. 3 assumes that initial SO_2 concentrations in the liquid droplets are negligible. Nonnegligible initial SO_2 concentrations should decrease τ values somewhat.

Acknowledgment

This article presents work that was common to research efforts supported by NSF, NASA, and the Rhône-Poulenc Basic Chemicals Company. Support from all of these organizations is therefore gratefully acknowledged.

Literature Cited

Aharon, I., and B. D. Shaw, ''Estimates of Liquid Species Diffusivities from Experiments on Reduced-Gravity Combustion of Heptane-Hexadecane Droplets,'' *Comb. Flame*, **113**, 507 (1998).

Albright, L. F., and E. G. Lang, ''Sulfuric Acid Recovery from Alkylation Units and Other Processes,'' *Encyclopedia of Chemical Processing and Design*, Vol. 55, J. J. McKetta, Executive Editor; G. E. Weismantel, Associate Editor, Marcel Dekker, New York (1996).

Bush, B. L., and G. Levine, ''The Generation and Management of Wastes and Secondary Materials in the Petroleum Refining Industry—1987–1988,'' *Haz. Waste Haz. Mat.*, **9**, 73 (1992).

Donovan, J. R., and J. M. Salamone, ''Sulfuric Acid and Sulfur Trioxide,'' *Encyclopedia of Chemical Technology*, 3rd ed., Vol. 22, M. Grayson, Executive Editor; D. Eckroth, Associate Editor, Wiley, New York (1978).

Green, G. J., F. Takahashi, D. E. Walsh, and F. L. Dryer, ''Aerodynamic Device for Generating Mono-Disperse Fuel Droplets,'' *Rev. Sci. Inst.*, **60**, 646 (1989).

Hayduk, W., H. Asatani, and B. C.-Y. Lu, ''Solubility of Sulfur Dioxide in Aqueous Sulfuric Acid Solutions,'' *J. Chem. Eng. Data*, **33**, 506 (1988).

Krasil'nikov, M. V., B. E. Shenfel'd, and V. S. Sushchev, ''Gas-Evolution Dynamics Upon the Thermal Decomposition of Spent Sulfuric Acid,'' *J. Appl. Chem. USSR*, **63**, 1032 (1990).

Krasil'nikov, M. V., B. E. Shenfel'd, and V. S. Sushchev, ''Oxidation of Organic Impurities in Decomposition of Spent Sulfuric Acid in a Fluidized Bed,'' *J. Appl. Chem. USSR*, **64**, 2056 (1991).

Müller, H., ''Sulfuric Acid and Sulfur Trioxide,'' *Ullman's Encyclopedia of Industrial Chemistry, 5th Completely Revised Edition*, Vol. A25, B. Elvers, S. Hawkins, and W. Russey, eds., VCH Verlagsgesellschaft Weinheim, Germany (1994).

Rubin, M. B., and R. M. Noyes, ''Measurements of Critical Supersaturation for Homogeneous Nucleation of Bubbles,'' *J. Phys. Chem.*, **91**, 4193 (1987).

Rubin, M. B., and R. M. Noyes, ''Thresholds for Nucleation of Bubbles of N_2 in Various Solvents,'' *J. Phys. Chem.*, **96**, 993 (1992).

Sigel, D., Virtual Visions Software, Cupertino, CA 95014 (1992).

Sung, S., G. Szechy, and L. F. Albright, ''Decomposition of Spent Alkylation Sulfuric Acid to Produce Sulfur Dioxide and Water,'' *Ind. Eng. Chem. Res.*, **32**, 2490 (1993).

Wang, D. F., and B. D. Shaw, ''Droplet Combustion in a Simulated Reduced Gravity Environment,'' *Comb. Sci. Tech.*, **113–114**, 451 (1996).

Manuscript received Nov. 17, 1997, and revision received Mar. 25, 1999.